Modeling of the resonant magnetic perturbation effect on detachment in the Large Helical Device

Modeling of the resonant magnetic perturbation effect on detachment in a large helical device

Mikhail Tokar[1,2], Masahiro Kobayashi[2,3] and the LHD Experiment Group

[1] Forschungszentrum Jülich GmbH, 52425 Jülich, Germany;
[2] National Institute for Fusion Science, National Institutes of Natural Sciences, 322-6, Oroshi-cho, Toki 509-5292, Japan;
[3] The Graduate University for Advanced Studies, SOKENDAI, Toki 509-5292, Japan.

Abstract. An approach to describe the plasma parameter variation with the effective minor radius across the edge region in the heliotron Large Helical Device (LHD) in configurations without and with a resonant magnetic perturbation (RMP) is elaborated, by averaging fluid equations for transport of particles, momentum and heat over the flux surfaces. Numerical solutions of one-dimensional, time-dependent equations derived and analytical estimates performed allow to interpret the LHD experiments on the density limit. Calculations reproduce qualitatively the principal difference between situations without and in the presence of RMP: in the former case a thermal collapse of the discharge occurs immediately after the plasma detachment from the divertor target plates at a radiation level of 0.4-0.5; in the latter one the radiating layer is localized at the plasma edge even if the power radiated exceeds 90% of the input one. The prominent role for such a behavior of plasma particle flows along magnetic field lines perturbed by RMP, leading to a positive radial gradient of the plasma density inside the magnetic island, is demonstrated.

1. Introduction

A power of 100 MW and higher is expected to be transferred into the divertor of future thermonuclear fusion reactors and handling of power loads onto divertor target plates is one of the most critical issues. The most modern engineering technologies presumes that a long enough life time of targets can be guaranteed if up to 90% of power, coming out of the confinement region, will be removed before the plasma contacts them [1]. One of the most promising ways to achieve this is to realize a state with the plasma detached from the target plates because the energy is mostly dissipated by the radiation of impurity particles from the plasma edge. Therefore the understanding of conditions and physical mechanisms of detachment and searching for possibilities to control reliably the strongly radiating edge region, being simultaneously compatible with a good enough confinement in the plasma core, is one of the most important tasks in fusion studies.

Although a significant progress in such investigations has been achieved on axis-symmetric tokamaks, being presently the most advanced concept for magnetic fusion, studies of detachment in helical devices [2,3] are also of importance for the reactor design. Since the magnetic field in helical systems is completely generated by currents in external coils, the field topology, its effects on the plasma transport and, in particular, on the plasma detachment conditions and characteristics, can be investigated, by varying the magnetic geometry in a wide range. One of very impressive findings in Large Helical Device (LHD) is the effect on the behavior of detachment and detached plasma, by applying a resonant magnetic perturbation (RMP) which generates at the very plasma edge a broad magnetic island centered at the resonant flux surface (RS) [4]. To some extend this is similar to the island divertor configuration realized in the stellarators W7-AS and W7-X.

Without RMP the increase of the plasma density to a critical level, where the radiated power approaches roughly to a half of the input one, leads to detachment from the divertortargets and uncontrollable spreading of the radiation zone to the plasma core, ending in a thermal collapse (TC) of the whole discharge. With the RMP even after detachment the impurity radiation is remaining localized at the plasma edge, in the region between the resonant magnetic surface and scrape-off layer boundary. By rising the plasma density the radiation level can be significantly increased before a TC is triggered. This behavior is demonstrated in figure 1 where the radiated power measured by bolometers is displayed as a function of the plasma line averaged density. On the one hand, the fact the RMP allows to initiate detachment at a lower plasma density and to get before TC states with the power radiated above 90% of the input one as shown in the present modeling, provides a promising approach to solve the problem of plasma-wall interaction in a fusion reactor. On the other hand, the RMP doesn't affect noticeably the collapse density limit (DL). To increase DL one can try in future to combine RMP operation with the injection of hydrogen isotope pellets. Recently it has been demonstrated that the latter permits to rise DL significantly [5].

Figure 2 shows typical profiles of the plasma parameters measured at the outer

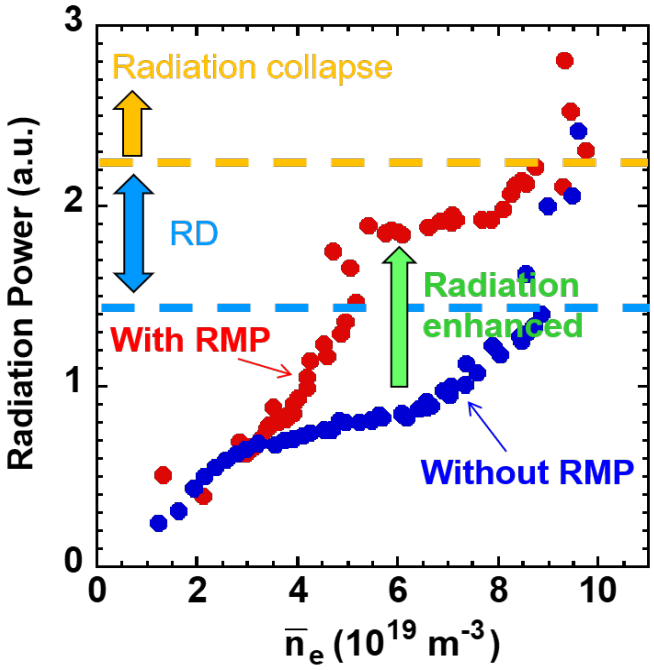

Figure 1. The radiated power versus the plasma line averaged density [8].

plasma in a typical high-density discharge in the LHD at stages without and with RMP. The behavior described above promises a robust approach to control detachment also for tokamaks devices, where recently RMP have been widely used to mitigate excessive divertor power load [6, 7] Thus the understanding of detachment features in helical devices like LHD is of general interest for magnetic fusion program.

In the present paper an approach is proposed to understand, interpret and model the impacts of RMP on detachment in the Large Helical Device. The reminder of the paper is structured as follows. In next section the basic equations used henceforth to describe the plasma components and magnetic geometry are introduced and one-dimensional equations for the variation of the plasma parameters in the direction across unperturbed flux surfaces are deduced. The results of calculations for the LHD without and with RMP are presented and compared with the experimental data in section 3. Conclusions are drawn in section 4.

2. Basic equations

2.1. Description of plasma components

The following set of transport equations [10] is applied to model the behavior of the plasma parameters in the LHD edge region with the magnetic island. Figure 3a shows the Poincare plots for the LHD magnetic configurations without and with the RMP of $m/n = 1/1$ helicity obtained, with field line tracing calculations in a vacuum approximation, i.e by neglecting plasma response against the RMP. In

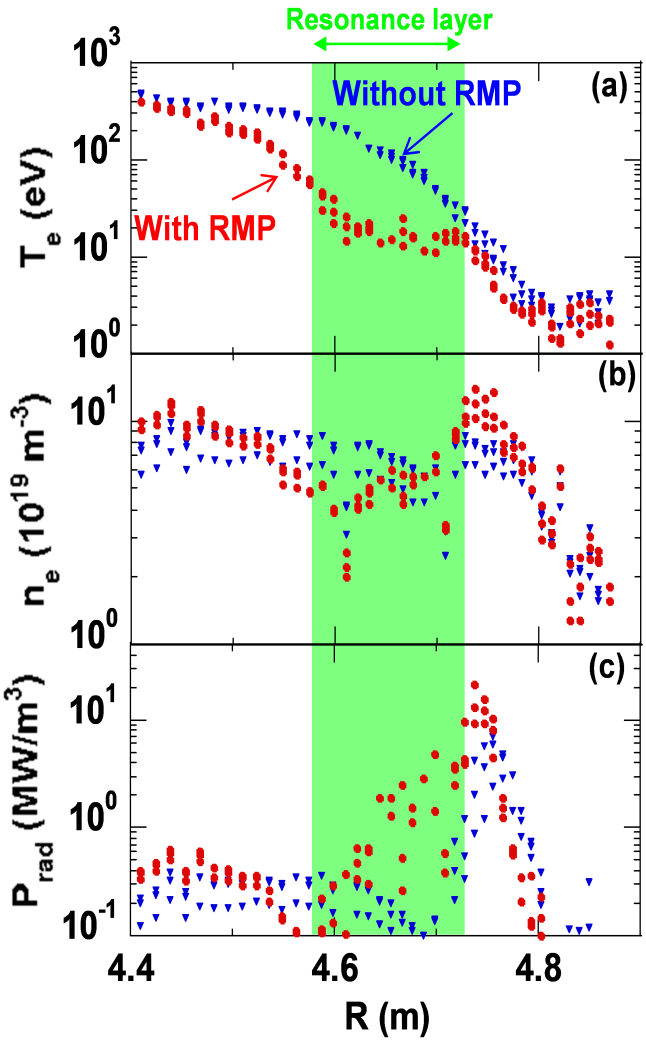

Figure 2. The profiles of the measured electron temperature (a), density (b) and radiation power density estimated for a carbon impurity concentration of 1% (c) at the outer edge of the LHD without (blue signs) and with (red signs) RMP [9].

figure 3b a schematic view of the plasma poloidal cross-section with the island, the coordinate system used and components of charged particle and heat flows parallel and perpendicular to the flux surfaces are demonstrated.

The density of plasma particles n is defined from the continuity equation:

$$\partial_t n + \nabla \cdot \mathbf{\Gamma} = S_p, \tag{1}$$

where $\mathbf{\Gamma} = \mathbf{b}_\perp \Gamma_\perp + \mathbf{b}_{||} \Gamma_{||}$ with $\mathbf{b}_{||}$ and $\mathbf{b}_\perp$being the components of the local unit vector, $\Gamma_\perp = -D_\perp \mathbf{b}_\perp \cdot \nabla n$ - the density of the plasma flux perpendicular to the magnetic field, $D_\perp$ - the plasma perpendicular diffusivity; the flux density along the magnetic field, $\Gamma_{||} = nV_{||}$, where $V_{||}$ is the plasma parallel velocity, is governed by the parallel momentum balance equation:

$$\partial_t \Gamma_{||} + \mathbf{b}_{||} \cdot \nabla \left(nc_s^2 \right) - \nabla \cdot \left[D_\perp \mathbf{b}_\perp \left(\mathbf{b}_\perp \cdot \nabla \Gamma_{||} \right) \right] = -S_m, \tag{2}$$

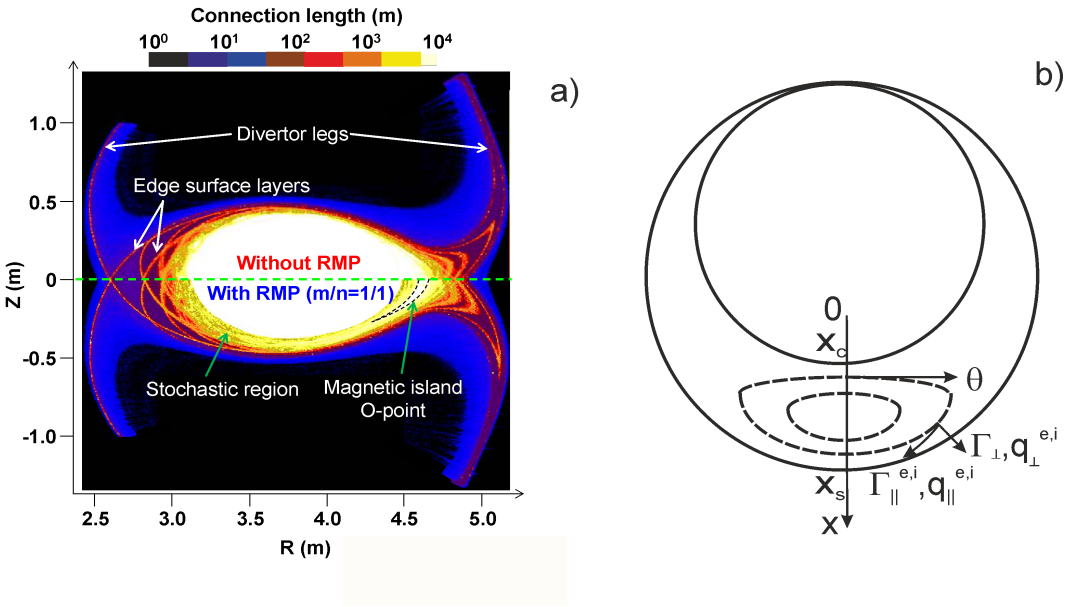

Figure 3. The Poincare plots for LHD magnetic configurations without and with the RMP (a) and a schematic view of the plasma poloidal cross-section with the island, the coordinate system used and components of charged particle and heat flows.

where $c_s = \sqrt{(T_e + T_i)/m_i}$ is the ion sound velocity, T_e and T_i are the temperatures of electrons and ions, respectively, m_i is the mass of the main ions.
The densities of the plasma component thermal energy, $W_{e,i} = 1.5nT_{e,i}$, are computed from the heat balance equations:

$$\partial_t W_e + \nabla \cdot \boldsymbol{q_e} = -K(T_e - T_i) - Q_{rad} - S_e, \tag{3}$$

$$\partial_t W_i + \nabla \cdot \boldsymbol{q_i} = K(T_e - T_i) - S_i \tag{4}$$

where $\boldsymbol{q_{e,i}} = q_{\perp e,i}\mathbf{b}_\perp + q_{||e,i}\mathbf{b}_{||}$ are the heat flux densities, with the parallel and perpendicular components:

$$q_\perp^{e,i} = 1.5\Gamma_\perp T_{e,i} - \kappa_\perp^{e,i}\mathbf{b}_\perp \cdot \nabla T_{e,i},\ q_{||}^{e,i} = 2.5\Gamma_{||} T_{e,i} - \kappa_{||}^{e,i}\mathbf{b}_{||} \cdot \nabla T_{e,i} \tag{5}$$

Here, $\kappa_\perp^{e,i}$ is the heat conductivity perpendicular to the magnetic field, and $\kappa_{||}^{e,i} = A_{e,i}T_{e,i}$ - the parallel heat conductivity with $A_e = 2.1 \times 10^{22}\beta_{HFL}$ and $A_i = 6.5 \times 10^{20} eV^{-2.5} m^{-1} s^{-1}$ for electrons and ions, respectively; the heat flux limit factor $\beta_{HFL} = 0.1$ takes into account the reduction of the parallel electron heat conduction [11] with respect to the usual Spitzer-Harm approximation [10]. The first terms on the right hand sides (r.h.s.) of equations (3,4) correspond to the heat transfer between electrons and ions by coulomb collisions; here $K = 3m_e n/(m_i \tau_{ei})$, with m_e being the electron mass and $\tau_{ei} \sim T_e^{1.5}/n$ - the e-i collision time [10]. The term $Q_{rad} = nL_I n_{imp}$ is the electron energy loss on impurity excitation, with L_I being the cooling rate, dependent on the electron temperature and computed in a non-coronal approximation, see [12], and n_{imp} - the total density of impurity ions of all charge states Z. The approach to calculate the radial profile of n_{imp} is outlined in the Appendix.

The last contributions in the r.h.s. of equations (1-4) are the sources/sinks of plasma particles, their momentum and energies:

$$S_p = k_{ion} n (n_0 + n_*),\ S_m = m_i k_{cx} n_0 \Gamma_{\|}, \tag{6}$$

$$S_e = k_{ion} n (n_0 + n_*) E_{ion},\ S_i = k_{cx} n_0 (W_i - n E_{fc}), \tag{7}$$

where k_{ion} and k_{cx} are the ionization and charge exchange (cx) rate coefficients; $E_{ion} \approx 30eV$ is the effective energy lost by electrons on the atom ionization assessed by including losses on the excitation; n_0 - the density of primary Franck-Condon atoms with the energy $E_{fc} \approx 3eV$ born by the dissociation of gas molecules in a very thin outer plasma layer, n_* - the density of "hot" atoms generated by cx-collisions of primary atoms with ions. By moving towards the plasma core n_0 decays according to the following continuity equation:

$$-V_0 \partial_r n_0 = -\left(k_{ion} + k_{cx}\right) n n_0, \tag{8}$$

where $V_0 = \sqrt{2E_0/(3m_i)}$ is the characteristic velocity of primary atoms; the density of cx-atoms is modeled in a diffusion approximation:

$$\partial_r \left(-D_{cx} \partial_r n_*\right) = n (k_{cx} n_0 - k_{ion} n_*), \tag{9}$$

with $D_{cx} = T_i / \left[m_i n \left(k_{ion} + k_{cx}\right)\right]$ being the diffusivity of cx-atoms; since in the LHD the poloidal cross-sections of surfaces are close to elliptic ones the effective radius of flux surfaces, $r = z\sqrt{E}$, with z being the minor half-width of the surface and E - its ellipticity.

2.2. Boundary conditions

The set of equations above has to be supplemented by boundary conditions. The inner boundary of the computation domain corresponds to the interface with the plasma core, $r = r_{core}$, where direct impacts of the edge magnetic island are negligible. Here, the particle and heat fluxes are prescribed:

$$r_{core}:\ \Gamma_\perp - V_0 n_0 - D_{cx} \partial_r n_* = \Gamma_c;\ q_\perp^{e,i} = q_c/2 \tag{10}$$

with the magnitudes of Γ_c and q_c defined by the particle and heat source in the plasma core due to neutral beams.

The outer border is defined by the scrape-off layer (SOL) formed by divertor legs, $r = r_{SOL}$. In the legs of the LHD the plasma density does not usually exceed $10^{19} m^{-3}$ [14,15] and, therefore, the particle sources and energy losses are negligible here and the plasma parameters change weakly along the legs. In particular, the parallel velocity is comparable with its value at the targets, which is, according to the Bohm's criterion, is equal c_s, i.e. the perpendicular component of the velocity is of $c_s \beta$ where $\beta = B_r/B_\phi \ll 1$. Thus for the densities of the particle and energy flows at the SOL border one has:

$$r = r_{SOL}:\ \Gamma_\perp = \beta n c_s,\ q_\perp^{e,i} = \gamma_{e,i} T_{e,i} \Gamma_\perp \tag{11}$$

where $\gamma_{e,i}$ are the sheath heat transmission coefficients for electrons and ions. The boundary condition for the continuity equation (6) of impurity ions are similar to those for equation (1).

For equation (8) the density of primary neutrals at $r = r_{SOL}$ is chosen to reproduce the required value of the plasma density at the plasma core boundary, $n\left(r_{core}\right) = n_c$; it is assumed that cx-atoms escape from the computation domain with their thermal velocity, i.e. $D_{cx}\partial_r n_* = \pm n_* \sqrt{T_i/m_i}$ are the boundary conditions for equation (9) at $r = r_{core}$ and $r = r_{SOL}$, with signs (+) and (−), respectively.

2.3. Magnetic geometry

By currents in a special coil a resonant magnetic perturbation (RMP) can be generated in the LHD. This provides a perpendicular component of the magnetic field, $B_r = \beta_{RMP} B_\phi \sin\theta$, where $\beta_{RMP} \approx 10^{-3}$ is the RMP relative amplitude and the phase $\theta = y/a$, with y being the distance from a particular field line on the resonant flux surface (RS) of the minor radius $r = r_{RS}$ where the rotation transform $\iota = (2\pi)^{-1}$. In the presence of the RMP the magnetic geometry is principally changed and instead of the unperturbed RS a magnetic island is formed [16] of the radial width $2\Delta = 4\sqrt{\frac{\beta_{RMP} R_{RS}}{|d\iota/dr|}}$, where R_{RS} is the RS major radius. Within the island field lines form closed flux surfaces nested around the island axis at $y = 0$. The cross-section of such a surface in a plane perpendicular to the island axis is described by the equation for the radial deviation from the RS, ξ :

$$\xi = \pm\sqrt{\xi_0^2 - \Delta^2 \sin^2\left(\theta/2\right)} \tag{12}$$

with ξ_0 being the maximum value of ξ at $y = 0$ for the flux surface in question. By moving along a field line within the island a radial shift at a distance up to 2Δ occurs and, therefore, the parallel transport of charged particles and heat contributes to the transport in the direction r across unperturbed magnetic surfaces. One of the important geometric characteristics is the angle α between the x-direction and the normal $\mathbf{b}_\perp$ to the flux surface; one can find that in a point with the coordinates x, y

$$\tan\alpha = \frac{d\xi}{dy} = \frac{\pm\Delta^2 \sin\theta}{4 r_{RS}\xi}. \tag{13}$$

2.4. One-dimensional approximation

In the present paper the global features of the magnetic island impact on the LHD plasma, such as the density limits for the onsets of detachment and RC, are mostly considered. For this purpose the equations above are reduced to one-dimensional (1D) ones under the following assumptions: (i) even in the presence of the island the plasma parameters change mostly in the radial direction r perpendicular to the unperturbed magnetic surfaces, (ii) the radial width of the calculation domain, $r_{SOL} - r_{core}$, is small compared to r_{SOL} and r_{core} and a slab approximation can be applied (iii) the electron

and ion temperatures are close each other as it is expected at the plasma edge by approaching to the density limit due to the increase of the heat transfer rate coefficient $K \sim n^2/T_e^{1.5}$. Therefore, henceforth, we introduce a single plasma temperature T and neglect components of the plasma parameter gradient other than $\partial_r(...)$. The densities of plasma particle and total heat fluxes in the r-direction are as are equal $\Gamma_r = \Gamma_{\perp r} + \Gamma_{||r}$ and $q_r = q^e_{\perp r} + q^i_{\perp r} + q^e_{||r} + q^i_{||r}$, respectively, where

$$\Gamma_{\perp r} = \Gamma_\perp \cos\alpha = \frac{-D_\perp \partial_r n}{1+\tan^2\alpha},\ \Gamma_{||r} = \Gamma_{||}\frac{B_r}{B_\phi} = \Gamma_{||}\beta_{RMP}\sin\theta,$$

$$q^{e,i}_{\perp r} = 1.5\Gamma_{\perp r}T - \frac{\kappa^{e,i}_\perp \partial_r T}{1+\tan^2\alpha},\ q^{e,i}_{||r} = 2.5\Gamma_{||r}T - \kappa^{e,i}_{||}\left(\beta_{RMP}\sin\theta\right)^2\partial_r T,$$

with α being the angle between the normal to the flux surface and the direction r; by moving along a surface in the island α changes from 0 at the surface point of the minimum x, being closest to the plasma axis, to π at the point where x is the maximum one.

1-D equations, describing the variation of parameters in the x-direction follow by averaging equations (1), (2), the sum of equations (3) and (4), and equation (6) over the RMP phase $0 \le \theta \le \pi$:

$$\partial_t n + \partial_r\left(G_r - D_{eff}\partial_r n\right) = S_p \tag{14}$$

$$\partial_t G_r - \mu\partial_r\left(D_{eff}\partial_r G_r\right) + 2\beta^2_{RMP}\varphi\partial_r\left(nc_s^2\right) = -k_{cx}n_0 G_r \tag{15}$$

$$3\partial_t\left(nT\right) - \partial_r\left[\kappa_{eff}\partial_r T + \left(3D_{eff}\partial_r n - 5G_r\right)T\right] = -S_e - S_i \tag{16}$$

$$\partial_t n_{imp} - \partial_r\left[D_{eff}\partial_r n_{imp} - \left(G_r/n + C\beta^2_{RMP}\varphi\partial_r T\right)n_{imp}\right] = k^0_{ion}nn^{imp}_0 \tag{17}$$

where $G_r = \left\langle \Gamma_{||}\sin\theta\right\rangle$ with $\langle\cdots\rangle$ denoting the average over the RMP phase; the effective radial transport coefficients

$$D_{eff} = \frac{D_\perp}{\gamma},\ \kappa_{eff} = \frac{\kappa^e_\perp + \kappa^i_\perp}{\gamma} + \left(\kappa^e_{||} + \kappa^i_{||}\right)\beta^2_{RMP}\varphi,$$

with $\gamma = \sqrt{1 + \left[\frac{\Delta^2}{4a(r-r_{RS})}\right]^2}$, $\varphi = \frac{\theta_r}{\pi} - \frac{\sin(4\theta_r)}{4\pi}$, $\theta_r = \arcsin\sqrt{1-\left(\frac{r-r_{RS}}{\Delta}\right)^2}$ and $\mu \lesssim 1$. A similar approach was used before [17, 18], by considering the RMP coupling to zonal flows through the parallel electric field.

It is interesting to note that $\gamma \to \infty$ and $D_{eff} \to 0$ by $r \to r_{RS}$, i.e. by approaching to the resonant surface. Physically this means that here the normal to the local flux surface is perpendicular to the radial direction. On the contrary the contribution of the parallel transport, being proportional to the factor φ, approaches its maximum at the RS and remains the only one to the effective radial transport here. From equation (15) one can see the parallel particle flow is driven by the plasma pressure gradient, in turn this is reduced through the flow. After several sound oscillations damped by the perpendicular momentum transfer and friction with neutrals a stationary state is established finally.

3. Results of calculations

The following input parameters have been used for calculations in the 1D approximation: the positions of the computation domain boundaries, $r_{core} = 0.576m$ and $r_{SOL} = 0.76m$, of the resonant surface $r_{RS} = 0.714m$, the island half-width $\Delta = 0.024m$; the density of the heat flux from the core $q_c = 80\,kW\,m^{-2}$; the perpendicular transport coefficients $D_\perp = 0.5m^2s^{-1}$, $\kappa_\perp = 2 \times 10^{20}m^{-1}s^{-1}$. Instead of an explicit modeling, by using equations (7) and (20), a typical concentration of carbon impurity n_{imp}/n of 0.01 has been fixed. Equations (17)-(19) have been solved numerically by the method outlined in [19] with a typical time step of $50\mu s$ and 201 equidistant grid point in the computations domain $r_{core} \leq r \leq r_{SOL}$.

Figure 4 shows the plasma temperature at the SOL boundary $T\left(r_{sol}\right)$ and the radiation level

$$\gamma_{rad} \equiv \frac{1}{q_c} \int\limits_{r_{core}}^{r_{SOL}} n L_I n_{imp} dr$$

versus the plasma density at the core border, n_c, controlled by the hydrogen gas density on the plasma boundary, $n_0\left(r_{SOL}\right)$, in configurations without and with the RMP. In the former case the parts of the dependencies marked by the pluses have the form typical for a bifurcation and the corresponding states have to be unstable from a general point of view. The fact that these states are obtained in the present calculations is explained by a not long enough calculation time and, by increasing this sufficiently, final indeed stationary states of extremely small $T_s = T\left(r_{sol}\right) \approx 0.1 - 0.2eV$ were got. This is demonstrated in figure 5a where the profile $T\left(x = r - r_{core}\right)$ is shown for 2 magnitudes of the core plasma density in the vicinity of its critical for the SOL detachment level n_{cr} of $5 \times 10^{19}m^{-2}s^{-1}$, differing by less than 1%, see figure 5b with the plasma density profiles. States of a very low $T\left(r_{sol}\right)$ are not fully realistic because some physical processes important under such conditions, e.g., recombination, are not included into the present model. The transition to such states, initiated as γ_{rad} exceeds a critical value 0.4, corresponds actually to a thermal collapse when the radiation zone uncontrollably penetrates towards the plasma core. This can be seen in figure 5c where the corresponding profiles of $Q_{rad}\left(r\right)$ are displayed. The picture of detachment in the LHD revealed above is essentially similar to the radial detachment in Ohmic discharges in the tokamak TEXTOR and the exhaustive analysis in [12, 20] can be principally applied here.

In the configuration with the RMP $T\left(r_{sol}\right)$ decreases and γ_{rad} increases monotonously as the plasma core density grows up with $n_0\left(r_{SOL}\right)$. Therefore no thermal collapse occurs even after the SOL detachment at $n_{cr} \approx 4.1 \times 10^{19}m^{-3}$, as one can see in figure 6 where the profiles of $T(x)$, $n(x)$ and $Q_{rad}(x)$ are presented for 3 magnitudes of n_c. The radiation layer stays always at the very plasma edge mostly in the region between the RS and SOL, see figure 6c. By increasing the neutral influx in order to rise n_c further the collapse of the profiles of all parameters considered takes place: the

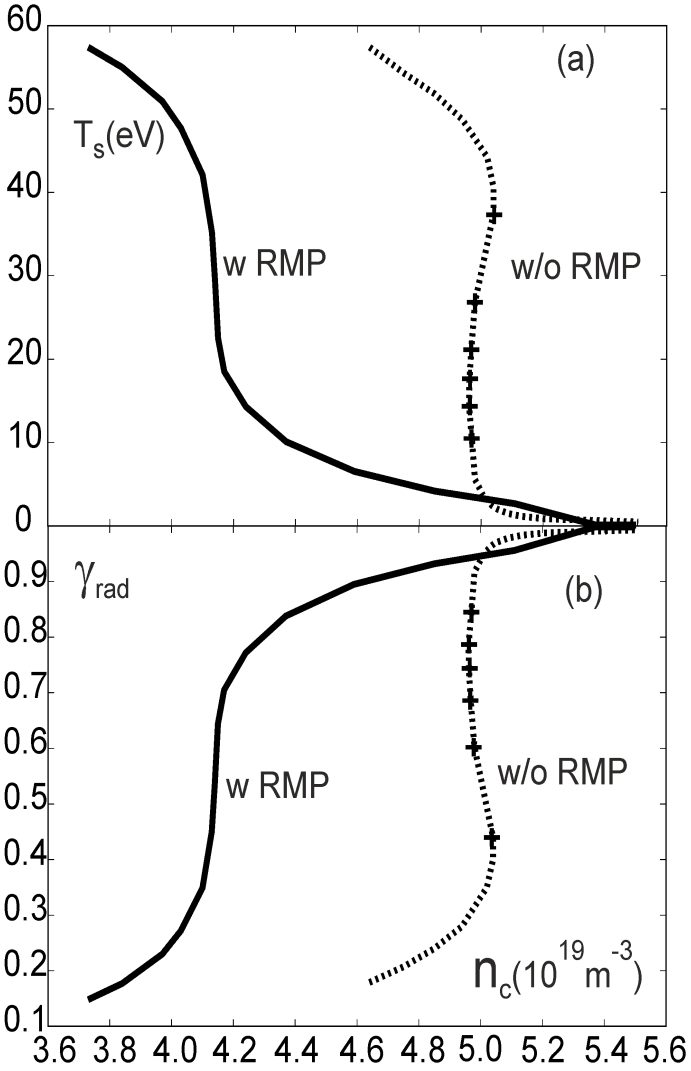

Figure 4. The temperature at the SOL-border, $T_s = T(r_{SOL})$ (a) and radiation level (b) versus the plasma density at the core border, n_c, calculated with (solid lines) and without (dotted lines) RMP impacts.

temperature drops in the whole computation domain, due to deeper penetration of neutrals a strong density maximum arises at the inner boundary $x = 0$ leading to a strongly peaked there radiation losses. This behavior can be interpreted as a thermal collapse but the present model is not sufficiently sophisticated to describe it firmly.

At a finite β_{RMP} parallel flows affect the transport in the r-direction both of heat and of charged particles. On the one hand, a finite plasma pressure gradient $\partial_r P \sim \partial_r (nc_s^2)$ generates the particle flux G_r, see equation (19), by leading to the decrease of $|\partial_r P|$ and formation in the island region of profiles with $\partial_r T < 0$ and $\partial_r n > 0$. It is a self-sustaining situation: since $Q_{rad} \sim n^2$ the energy loss is higher in the outer island-half, therefore $\partial_r T$ becomes more negative and, consequently, $\partial_r n$ increases. This development is terminated as the plasma temperature drops to the level of several electron-volts and impurity cooling rate L_I begins to decrease. On the other

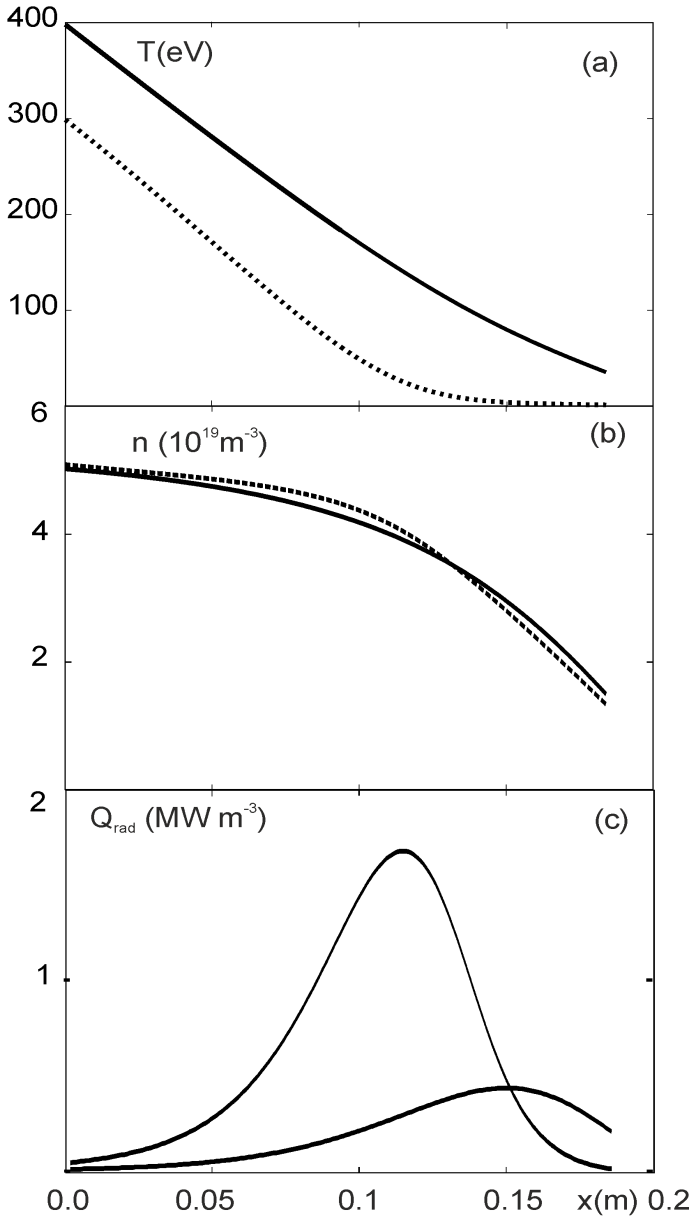

Figure 5. The profiles of the plasma temperature (a), density (b) and radiated power density (c) calculated without RMP impacts for 2 slightly different magnitudes of n_c; $x = r - r_{core}$.

hand, with RMP the parallel heat conduction $\kappa_{||} \sim T^{2.5}$ contributes to κ_{eff}, by making it larger and dependent on the plasma temperature. As it was demonstrated [12] such a modification affects the threshold of detachment in limiter tokamaks like TEXTOR and may be of importance for the LHD conditions. To investigate the relative importance of modifications induced by the RMP in the transport of particles and heat, calculations have been performed by applying the finite $\beta_{RMP} = 10^{-3}$ either in equation (19) and D_{eff} or in κ_{eff} only. If the RMP impact on the particle transport is taken into account the results are only slightly different from those found with the complete model above. In the case of modifications induced in the effective heat conduction no RMP effect is

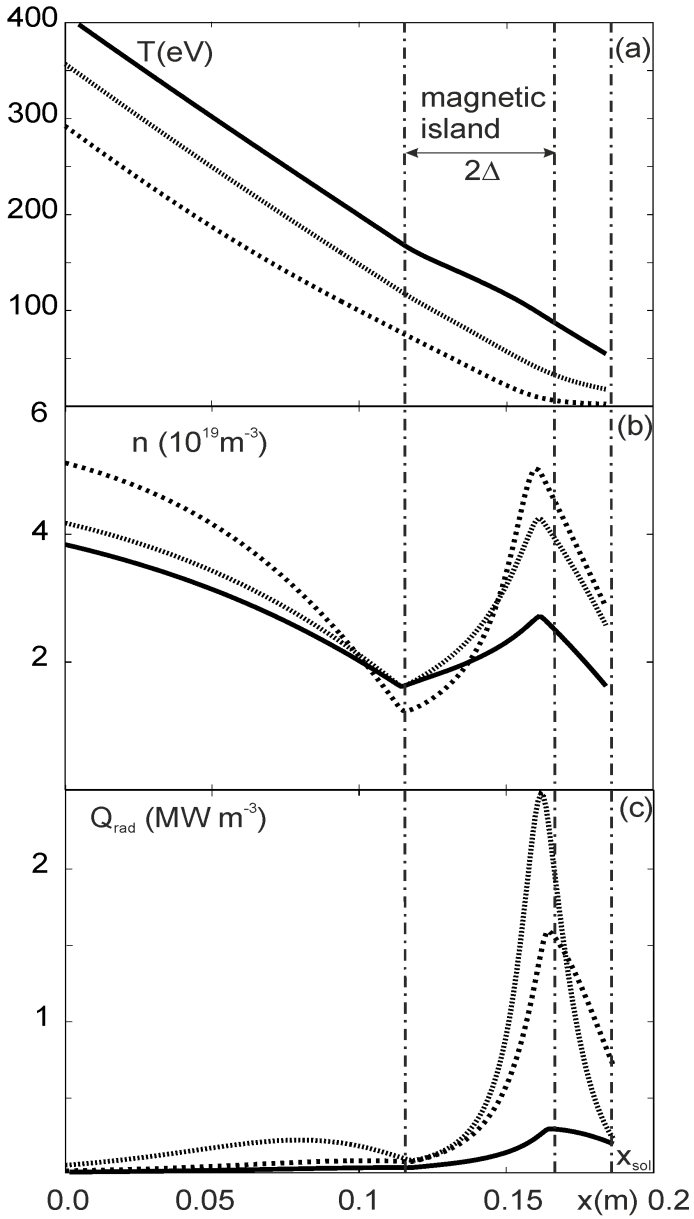

Figure 6. The profiles of the plasma temperature (a), density (b) and radiated power density (c) calculated with $\beta_{RMP} = 10^{-3}$ for 3 values of n_c.

seen: the SOL detachment at $\gamma_{rad} \approx 0.4$ leads to a thermal collapse. Thus changes induced in the particle transport, leading to non-monotonous plasma density profiles, with $\partial_x n > 0$ in the magnetic island, are decisive for the stabilizing effect of RMP on the detachment in the LHD.

4. Qualitative analytical analysis

To elucidate futher the mechanisms for the radiation layer stabilization by the RMP a very simplified model for the heat transport at the plasma edge with and without magneic island is considered in this section. This model includes the momentum balance

in the island in the simplest form of the pressure constancy:

$$n\left(x\right)T\left(x\right)=\text{const}=n_cT_c$$

with the prescribed density n_c at the interface of the island with the plasma core, $x=x_c$, and the plasma temperature T_c determined below;
the heat balance equation inside magnetic island taking into account the parallel heat conduction only:

$$\frac{d}{dx}\left(-\beta_{RMP}^2A_{||}T^{2.5}\frac{dT}{dx}\right)=-c_In^2L_I=-c_In_c^2T_c^2\frac{L_I}{T^2} \tag{18}$$

By multiplying the latter with $2T^{2.5}\frac{dT}{dx}$, one gets:

$$\frac{d}{dx}\left(\beta_{RMP}^2A_{||}T^{2.5}\frac{dT}{dx}\right)^2=2UT_c^2\sqrt{T}L_I\frac{dT}{dx}$$

where $U=\beta_{RMP}^2A_{||}c_In_c^2$.

For the present analysis we fix both boundary conditions for equation (22) at the outer island border, $x_s=x_c+2\Delta:\ T=T_s,\ -\beta_{RMP}^2A_{||}T^{2.5}\frac{dT}{dx}=-\kappa_\perp\frac{T}{\delta_T}$. An integration provides:

$$-\beta_{RMP}^2A_{||}T^{2.5}\frac{dT}{dx}=\sqrt{\left(\kappa_\perp T_s/\delta_T\right)^2+2UT_c^2g}$$

with

$$g\left(T_s,T\right)=\int\limits_{T_s}^{T}\sqrt{\Theta}L_Id\Theta$$

By integrating once more, we get an integral equation for the temperature profile:

$$\int\limits_{T_s}^{T(x)}\frac{\Theta^{2.5}d\Theta}{\sqrt{\left(\kappa_\perp T_s/\delta_T\right)^2+2UT_c^2g\left(T_s,\Theta\right)}}=\frac{2\Delta+x_c-x}{\beta_{RMP}^2A_{||}}$$

and a transcendent one for the core temperature T_c:

$$\int\limits_{T_s}^{T_c}\frac{T^{2.5}dT}{\sqrt{\left(\kappa_\perp T_s/\delta_T\right)^2+2UT_c^2g\left(T_s,T\right)}}=\frac{2\Delta}{\beta_{RMP}^2A_{||}}$$

Physically, in a steady state the heat flux from the core, $-\beta_{RMP}^2A_{||}T^{2.5}\frac{dT}{dx}\left(x=x_c\right)$, is compensated by the total heat loss from the island with the conduction through the outer border and impurity radiation

$$q_{loss}=\sqrt{\left(\kappa_\perp T_s/\delta_T\right)^2+2UT_c^2g\left(T_s,T_c\right)}$$

For the level of radiation losses one has:

$$\gamma_{rad}=1-\frac{\kappa_\perp T_s}{\delta_Tq_{loss}}$$

Stationary states are defined from the island heat balance

$$q_{loss}=q_{heat}$$

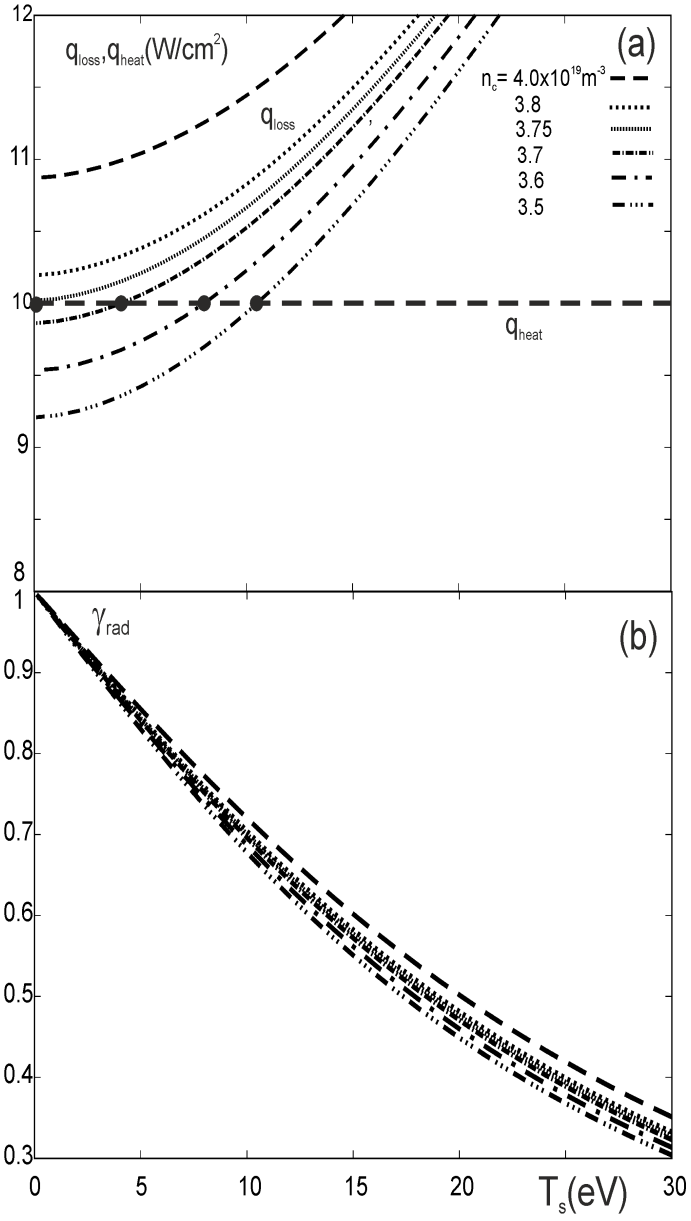

Figure 7. The total energy loss from the island with heat conduction and impurity radiation (a) and the radiation level (b) vs. the temperature at the island outer border for different values of the density at the interface with the plasma core, n_c; steady states are defined by the balance between q_{loss} and the heat influx into the island $q_{heat} = 10W\ m^{-3}$.

The dependencies $q_{loss}\,(T_s)$ and $\gamma_{rad}\,(T_s)$ for different n_c are presented in figure 7. With $q_{heat} = 10W/cm^2$ steady states exist for $n_c \leq n_{cr} \approx 3.75 \cdot 10^{19} m^{-3}$; for higher n_c there is no thermal equilibrium and a thermal collapse has to occur. The steady states, in which γ_{rad} can exceed 0.95, are stable. Indeed, the stability condition [12]:

$$\frac{dq_{loss}}{dT_\Delta} \sim \frac{d\ln q_{loss}}{d\ln T_\Delta} > 0$$

is satisfied for all cases. This situation is different to the one without RMP considered

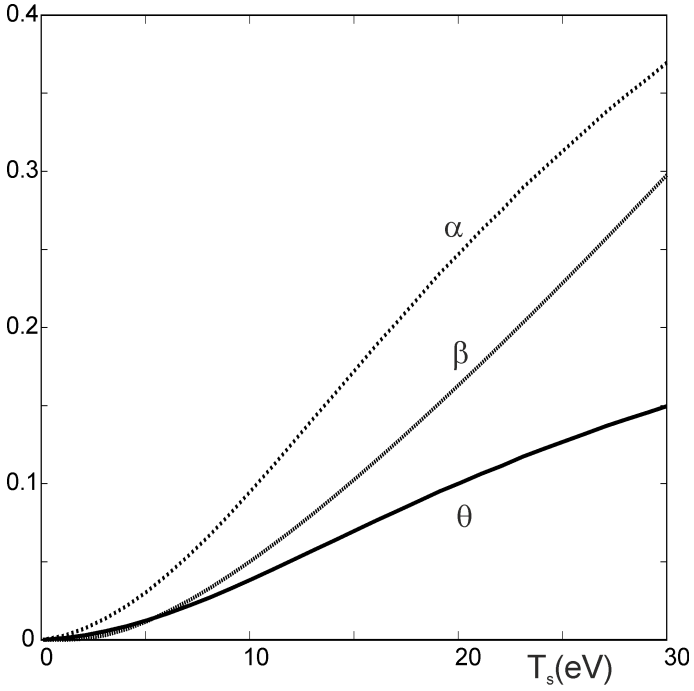

Figure 8. The dependencies of θ, α and β on T_s for $n_c = n_{cr} \approx 3.75 \cdot 10^{19} m^{-3}$.

below and in [12] for a limiter tokamak. To understand the behavior with the RMP we analyze the dependence of $d \ln q_{loss}/d \ln T_s$ on T_s. One can get:

$$\frac{d \ln q_{loss}}{d \ln T_s} = (1 - \gamma_{rad})^2 + \frac{U T_c^2 g(T_s, T_c)}{q_{loss}^2} (\alpha - \beta)$$

with

$$\alpha = \theta \left[2 + \frac{T_c^{1.5} L_I(T_c)}{g(T_s, T_c)} \right], \ \beta = \frac{T_s^{1.5} L_I(T_s)}{g(T_s, T_c)}, \ \theta = \frac{d \ln T_c}{d \ln T_s}$$

Figure 8 shows dependencies of θ, α and β on T_s for $n_c = n_{cr}$.

Thus, the effect of impurity radiation on stability is defined by the sign of the difference $\alpha - \beta$. In the T_s-range of interest this difference is always positive, see figure 8, and the radiation losses are not destabilizing. Qualitatively one can explain this as follows. Consider a spontaneous drop of T_s. If T_c would be independent of T_s, by meaning $\theta, \alpha = 0$, this should lead to the plasma density increasing according to the local law $n(x) \sim 1/T(x)$. As a result Q_{rad} will grow as $1/T_s^2$ and instability develops if γ_{rad} is large enough. However, not T_c but the heat influx into the island from the core is fixed. As a result, T_c somewhat decreases and n does not grow so strongly with droping T_s. Formally this is revealed through $\theta > 0$ and, thus, $\alpha > 0$. In addition, because $\theta < 1$ the radial gradient of $T(x)$ increases with diminishing T_s, the stronger the closer to the outer island boundary $x = x_s$, since $\kappa_{||} \sim T^{2.5}$. Therefore the regions with the largest increase in the plasma density are becoming less extended in the radial direction. This is mimicked in the decrease of β with T_s. Note the same argumentaion is relevant by explaining why the Q_{rad} peak becomes narrower with decreasing T_s, see figure 6c: the

smaller T_s the larger temperature gradient, figure 6a, the more $n(x)$, figure 6b, and, thus, $Q_{rad} \sim n^2$, are peaked in the island.

Consider now the situation without RMP. The heat balance equation in this case,

$$\frac{d}{dx}\left(-\kappa_\perp \frac{dT}{dx}\right) = -c_I n^2 L_I,$$

is treated, by assuming for clarity both $\kappa_\perp$ and n indpendent of x. Similarly to the analysis above we get for the total heat loss from the edge with heat conduction and radiation:

$$q_{loss} = \sqrt{\left(\frac{\kappa_\perp T_s}{\delta_T}\right)^2 + 2\kappa_\perp c_I n^2 \int\limits_{T_s}^{T_c} L_I dT}$$

Without RMP the width of the radiation layer is not related to that of the island. Therefore the value of the T_c is restricted from above by the requirement only that it is reached at the plasma periphery. According to the measurements [4] one can assume $T_c \approx 300eV$. For the temperature dependence [12] assumed in the present study

$$L_I = L_I^{\max} \exp\left[-\left(\sqrt{\frac{T}{T_2}} - \sqrt{\frac{T_1}{T}}\right)^2\right],$$

$T_c \gg T_2 \approx 60eV \gg T_1 \approx 5eV$ in the case of carbon impurity under consideration. Thus, the integral in the relation above is very weakly dependent on the upper limit and one gets:

$$\frac{d\ln q_{loss}}{d\ln T_s} = (1-\gamma_{rad})^2 - \frac{\kappa_\perp c_I n^2 T_s L_I(T_s)}{q_{loss}^2}$$

Thus, impurity radiation losses are always destabilizing and $d\ln q_{loss}/d\ln T_s$ can become negative by approaching of γ_{rad} to 1 for small enough T_s.

5. Conclusions

Time dependent one-dimensional transport equations to model the dependence on the effective minor radius of the plasma parameters averaged in the poloidal and toroidal directions are deduced by taking into account the presence of resonant magnetic perturbations at the plasma edge of the LHD. Calculations reproduce qualitatively the modifications of the plasma parameters and of the plasma behavior after detachment induced by the RMP: the generation inside the magnetic island of the plasma density profile with the positive radial gradient and stabilization of the layer where the impurity radiation losses are mostly localized at the plasma edge up to the loss power above 90% of the input one. This differs principally from the behavior without RMP where a thermal collapse and the plasma termination sets in immediately after the detachment from the SOL at a radiation level of 40-50%. Although the RMP affects both heat and particle transport in the magnetic island, where the strong parallel transport contributes to the effective radial one, namely the latter, leading to the inverted profile of the plasma

density, is decisive for the radiation zone stabilization. Up to now the calculations did not reveal usually expected strong flattening of the temperature profile within the island; this aspect has to be elaborated deeper in the future.

The 1D model elaborated in the present paper is not appropriate to reproduce important features of the RMP influence. A 2D modeling approach proposed and numerically realized in [21] allows to demonstrate in calculations many characteristics experimentally observed in the LHD configuration with the RMP. In particular, it is possible to reconstruct in 2D computations the concentration of impurity radiation losses in the vicinity of the magnetic island X-point, where finally a thermal collapse is initiated. These study is an intermediate step between the 1D consideration above to 3D simulations with the code suite EMC3-EIRENE applied normally to model the plasma edge in heliotrons, in particular, in the LHD [22]. It is planned to perform necessary developments in the code EMC3-EIRENE and to start in a near future 3D plasma simulations of the LHD discharges with the RMP. Such simulations are important to put a firm solid basis for the implementation of the RMP concept in future heliotron fusion reactors.

Acknowledgment

This work was partly supported by the JSPS KAKENHI grant no. 19H01878.

References

[1] N. Asakura et al., Nucl. Fusion **57**,126050 (2017)
[2] Y. Takeiri et al., Nucl. Fusion **58**, 106028 (2018).
[3] R.C. Wolf et al., Nucl. Fusion **57**,102020 (2017).
[4] M. Kobayashi et al., Nucl. Fusion **59**,096009 (2019).
[5] G. Fuchert et al., Increasing the density in W7-X: benefits and limitations, FEC 2018 Conf, IAEA, Gandhinagar, p. EX/3 (2018); https://www.iaea.org/sites/default/files/18/10/cn-258-abstracts.pdf.
[6] T.E. Evans et al., Nucl. Fusion **53**,093029 (2013).
[7] O. Schmitz et al., Nucl. Fusion **56**,066008 (2016).
[8] M. Kobayashi et al., 24th IAEA Fusion Energy Conference IAEA CN-197 San Diego, USA 8-13 Oct. 2012, EX/4-4.
[9] M. Kobayashi et al., Nucl. Fusion **53**,093032 (2013)
[10] S.I. Braginskii, Transport Processes in a Plasma, in *Reviews of Plasma physics*, Ed. M.A. Leontovich, Consultants Bureau, New York, Vol.**1**, 205-304 (1965).
[11] R.C. Malone, Phys. Rev. Lett. **34**, 721 (1975).
[12] M.Z. Tokar, Phys. Plasmas **7**, 2432 (2000).
[13] P.C. Stangeby, The Plasma Boundary of Magnetic Fusion Devices, IOP Publishing, London, 2000.
[14] S. Masuzaki et al., Nuclear Fusion **42**, 750 (2002).
[15] M. Kobayashi et al., Fusuion Science and Technology **58**, 220 (2010).
[16] G. M. Zaslavsky, Stochasticity of Dynamical Systems, Nauka, Moscow, 1984.
[17] D. Reiser and Chandra, Phys. Plasmas **16**, 042317 (2009).
[18] Leconte and Kim, Phys. Plasmas **22**, 082301 (2015).
[19] M.Z. Tokar, Modeling of profile evolution by transport transitions in fusion plasmas, in *Two Phase Flow, Phase Change and Numerical Modeling*, Ed. A. Ahsan, IntechOpen Limited, London, Chapter 7, 149 (2011); https://www.intechopen.com/books/two-phase-flow-phase-change-and-numerical-modeling/modelling-of- profile-evolution-by-transport-transitions-in-fusion-plasmas.
[20] M.Z. Tokar, Plasma Phys. Contr. Fusion **36**, 1819 (1994).
[21] M.Kobayashi and M.Z. Tokar, "Time-dependent plasma transport simulation for the study of edge impurity radiation dynamics with magnetic island in large helical device", Contributions to Plasma Physics, in press (https://doi.org/10.1002/ctpp.201900138).
[22] M. Kobayashi et al., Nuclear Fusion. **55**, 104021 (2015).

Appendix

An equation for the impurity ion density n_{imp} follows from the summation of continuity equations over all charge states Z:

$$\partial_t n_{imp} + \boldsymbol{\nabla} \cdot \boldsymbol{\Gamma}_{imp} = k^0_{ion} n n^0_{imp}$$

where $\boldsymbol{\Gamma}_{imp} = n_{imp} V_{imp\|} \mathbf{b}_{||} - D_\perp \left(\mathbf{b}_\perp \cdot \nabla n_{imp}\right) \boldsymbol{b}_\perp$ is the impurity ion flux density, with the parallel velocity of impurity assessed from the balance of the friction and the thermal forces [13], $V_{imp\|} = V_\| + C\mathbf{b}_{||} \cdot \nabla T_i$, $C \approx 3.2 \times 10^{12} T_i^{1.5} / \left(n\sqrt{m_i}\right)$; k^0_{ion} is the ionization rate coefficient of impurity neutrals and their density n^0_{imp} is determined from the continuity equation:

$$-V^0_{imp} \partial_r n^0_{imp} = -k^0_{ion} n n^0_{imp},$$

where $V^0_{imp} = \sqrt{2E^0_{imp}/(3m_{imp})}$ is the velocity of impurity atoms.

At the SOL boundary, $r = r_{SOL}$, the influx of impurity neutrals is defined by their erosion at the divertor targets by the main ions, $V^0_{imp} n^0_{imp} = Y\Gamma_\perp$, with the rate coefficient Y dependent, as well as the impurity atom energy E^0_{imp}, on the erosion mechanism. In the case of carbon sputtering $E^0_{imp} \approx 3eV$; Y is a function both of the energy of the main ions impinging the targets (physical sputtering) and of the temperature of the target surface (chemical sputtering). Both contributions to Y are reduced by the plasma detachment.